Journal of New Materials for Electrochemical Systems 21, 051-056 (2018)

Synthesis and Characterization of $Li(Li_{0.05}Ni_{0.6}Fe_{0.1}Mn_{0.25})O_2$ Cathode Material for Lithim Ion Batteries

A. Nichelson[1,2], S. Thanikaikarasan[3,*], K. Karuppasamy[4], S. Karthickprabhu[5], T. Mahalingam[6], X.Sahaya Shajan[1,†] and Edgar Valenzuela[7]

[1]Centre for Scientific and Applied Research, PSN College of Engineering and Technology, Tirunelveli-627 152, Tamil Nadu, India.
[2]St. Mother Theresa Engineering College, Vagaikulam, Mudivaithanenthal Post, Thoothukudi, Tamil Nadu 628 102, India
[3]Department of Physics, Saveetha School of Engineering, Saveetha University, Thandalam – 602105, Chennai, Tamil Nadu, India.
[4]Division of Electronics and Electrical Engineering, Dongguk University-Seoul, Seoul 04620, South Korea
[5]K.Ramakrishnan College of Technology, Samayapuram, Trichy-621 112
[6]Department of Physics, Alagappa University, Karaikudi 630 003, Tamil Nadu, India
[7]Facultad de Ingeniería, UABC Mexicali, 21280, México.

Received: October 31, 2017, Accepted: January 22, 2018, Available online: April 18, 2018

Abstract: *A new type of lithium enriched cathode material Li $(Li_{0.05}Ni_{0.6}Fe_{0.1}Mn_{0.25})O_2$ was synthesized by sol-gel method with citric acid as a chelating agent. The structural and morphological studies were systematically investigated through X-ray diffraction, SEM with EDS, FT-IR and Raman analyses. The crystallite size of the Li $(Li_{0.05}Ni_{0.6}Fe_{0.1}Mn_{0.25})O_2$ cathode material was found to be 45 nm thereby leads to the feasible movement of lithium ion all through the material. FT-IR spectroscopy was used to confirm the metal-oxygen interaction in the prepared cathode material. The electrical properties of the Li $(Li_{0.05}Ni_{0.6}Fe_{0.1}Mn_{0.25})O_2$ cathode material were studied by impedance and dielectric spectral analyzes. Li $(Li_{0.05}Ni_{0.6}Fe_{0.1}Mn_{0.25})O_2$ showed a maximum ionic conductivity of 10^{-6} S/cm at ambient temperature.*

Keywords: Sol-gel synthesis, $Li(Li_{0.05}Ni_{0.6}Fe_{0.1}Mn_{0.25})O_2$, nanoparticles, lithium ion batteries

1. INTRODUCTION

In recent years, rechargeable lithium ion batteries (LIBs) have received a great deal of attention due to their widespread potential applications in portable electronic devices which includes cellular phones, digital cameras, laptops, electric grids and hybrid electric vehicles [1-6]. As LIBs are the primary source of portable electrochemical energy storage, improving battery performance as well as reducing capital cost would pave the way to enable new technologies and expand their application widely. Usually, LIB prototype comprises of graphite or metallic lithium as negative electrode (anode) and transition-metal oxides (TMO) as positive electrode (cathode), separated by the electrolyte that provides a transport medium for ions. Amongst, positive electrode or cathode materials are of particular interest and a great volume of research in LIBs so far has been focused in cathode materials. This may be due to its higher rate capability, higher charge capacity, and (for cathodes) sufficiently high voltage can improve the energy and power densities of LIBs and make them smaller and cost effective.

The migration of lithium ions highly depends on the crystal structure of the cathode material. So far, different crystallite structures of cathode materials had been reported which include olivine [7], layered [5] and spinel phased structure [6]. $LiMn_2O_4$ with spinel structure (space-group: Fd3m) has attracted as a cathode material for Li-ion batteries due to their lower cost and lower toxicity than commercialized $LiCoO_2$. $LiMn_2O_4$ is safer than $LiCoO_2$ but has a lower capacity (110 mAh/g). Capacity loss is observed due to dissolution of manganese ($LiMn_2O_4$) in electrolyte [5, 7]. In a similar manner, in the case of olivine structured cathode material which include $LiFePO_4$, $LiMnO_2$ has numerous advantages but the iron and Mn based olivine intercalants are low energy producers compared to Ni and Co compounds[7]. Among layered cathode

To whom correspondence should be addressed:
Email:*sthanikai@rediffmail.com, †shajan89@gmail.com

materials they have shown a great battery performance due to their high discharge capacity, high electrical conductivity and capacity retention [8,9,10]. Among the layered oxides, $LiCoO_2$ was the first material which was investigated and implemented as cathode material for LIBs and the LIBs with $LiCoO_2$ as cathode and graphite as anode have been developed at a high level. However, the cell performance approaches a critical value which indeed need some innovations in the materials, both in preparation and performance [11,12] . Meanwhile, its low thermal stability and high cost is the main barrier for large sized cells in hybrid–electric vehicles (HEV). In order to overcome the above said drawbacks, scientific communities paid much attention towards the combined metal oxides based cathodes having 3d transition state $LiMO_2$ (M=Co, Ni, Mn).

Recently, the lithium–nickel-manganese-cobalt oxides (LNMCs) are highly fascinating and it shows high significance in LIBs because of their capacity and capacity retention[11]. Some of the important layered oxide cathode materials reported elsewhere are listed herein. Ohzuku and his co-workers have done a systematic study on $LiNi_{1/3}Co_{1/3}Mn_{1/3}O_2$ [9, 13, 14]. Later on, various stoichiometric ratios of LNMC have been studied. The Zn-doped $LiCo_{0.3}Ni_{0.4-x}Mn_{0.3}Zn_xO_2$ cathode materials have been synthesized via co-precipitation method by Chen et al and they found that $LiCo_{0.3}Ni_{0.4-x}Mn_{0.3}Zn_xO_2$ had stable layered structure with α-$NaFeO_2$ type with x up to 0.05. Also, Titanium doped cathode material $LiNi_{0.8}Co_{0.2-x}Ti_xO_2$ ($0 \le x \le 0.1$) powders with a high tap density have been successfully prepared by Tang et al[15]. Effect of carbon coating on the surface of $LiNi_{1/3}Co_{1/3}Mn_{1/3}O_2$ particles provides additional benefit to the material[16]. The substitution of elements such as Al, Fe, Ga, Cr, Mg, Ti instead of cobalt in Lithium manganese nickel cobalt oxide also showed favorable results[17].

In the present study, the Li $(Li_{0.05}Ni_{0.6}Fe_{0.1}Mn_{0.25})O_2$ compound has been prepared by citric acid assisted modified sol-gel method. Mostly, the substitution of cobalt for nickel results in an improved structure and electrochemical properties of the compound [18]. The chelating agents like citric acid act on nitrate ions to decompose it and the heat evolved from the decomposition of nitrate is utilized to decompose the remaining organic constituents [19]. The cathode material $Li(Li_{0.05}Ni_{0.6}Fe_{0.1}Mn_{0.25})O_2$ prepared by sol-gel method has been subjected to X-ray diffraction (XRD), Scanning electron microscopy (SEM), Fourier Transform Infrared Spectroscopic analysis (FTIR), Energy dispersive analysis by X-rays (EDX), conductance and dielectric spectra analyzed using Electrochemical Impedance Spectroscopy (EIS). The observed results were discussed and reported herein.

2. EXPERIMENTAL DETAILS

The AR grade precursor materials were purchased from Merck and used as such which includes lithium nitrate ($LiNO_3$), manganese Nitrate $Mn(NO_3)_2.6H_2O$, nickel Nitrate $(Ni(NO_3)_2.6H_2O$, iron III nitrate $Fe(NO_3)_3\,9H_2O$ and Citric acid ($C_6H_8O_7$). The cathode material $Li(Li_{0.05}Ni_{0.6}Fe_{0.1}Mn_{0.25})O_2$ was prepared by sol-gel method. The precursor materials were dissolved in distilled water and stirred vigorously for 7h. Afterward, citric acid, a chelating agent, was added drop wise to the reaction mixture. The pH of the solution was maintained between 6 and 7 by the addition of ammonium hydroxide. The pH maintained solution was then heated to 80 ˚C under continuous stirring to form a gel and it was preheated to 500 ˚C for 4 h. The obtained powder was grounded well for 2 h and again calcined at 950 ˚C for 15 h.

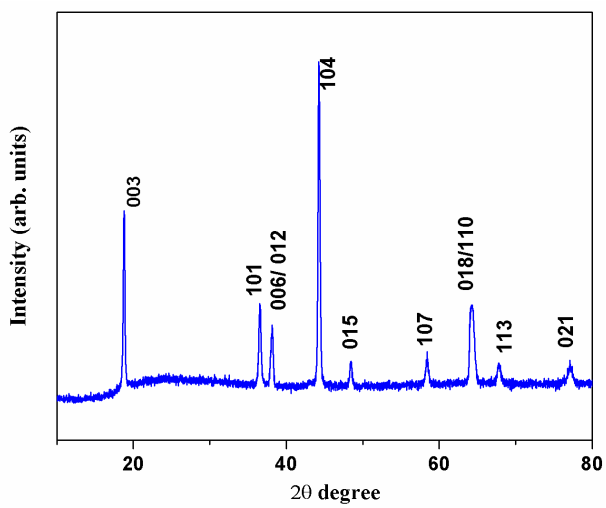

Figure 1. XRD pattern of $Li(Li_{0.05}Ni_{0.6}Fe_{0.1}Mn_{0.25})O_2$

The powder X-ray diffraction (PANalytical-XPERT PRO, Netherlands) measurement using CuKα radiation was employed to characterize the synthesized material. The morphological behavior and elemental analysis were done using SEM analyzer (JEOL-JSM.6400 with acceleration voltage of 5 kV). The FTIR spectrum was recorded using JASCO FTIR/4100 spectrophotometer (Japan) in the region 400-1100 cm^{-1} at room temperature with a signal resolution of 8 cm^{-1}. The Raman spectra were recorded by Laser Raman Spectroscopy with RENISHAW via Raman microscope using the 514 nm line of Argon laser source. Ionic conductivity measurements were carried out using impedance analyzer (Zahner IM6 Electrochemical Workstation (Germany)) in the frequency and temperature range of 100 mHz - 100 kHz and 303 K - 403 K respectively.

3. RESULTS AND DISCUSSION

3.1. Microstructural analysis

The XRD pattern of $Li(Li_{0.05}Ni_{0.6}Fe_{0.1}Mn_{0.25})O_2$ calcined at 950 ˚C is shown in Figure 1. The diffraction peaks observed is matched with the corresponding pattern of hexagonal α–$NaFeO_2$ structure with a space group of R $\bar{3}$ m (166), which includes the alternate layers of Li atom and MO_6 octahedra (M=Ni,Fe,Mn) indicating pure phase layered crystal structure [20]. Kim et al reported the peak splitting observed near 38˚ (006/012) and 65˚ (018/110), which shows that the layered structure is well developed [21]. The lattice constants were measured as a = 2.8963 Å, c= 14.1628 Å and c/a ratio is 4.889 Å, also the volume of the unit cell is V= 102.8 $Å^3$. The value of interplanar spacing d_{hkl} is calculated using Bragg's relation, which is given below in Eq (1).

$$d_{hkl} = \frac{\lambda}{2sin\theta} \quad (1)$$

The value of lattice parameters 'a' and 'c' are calculated using the below mentioned Eq (2) [22].

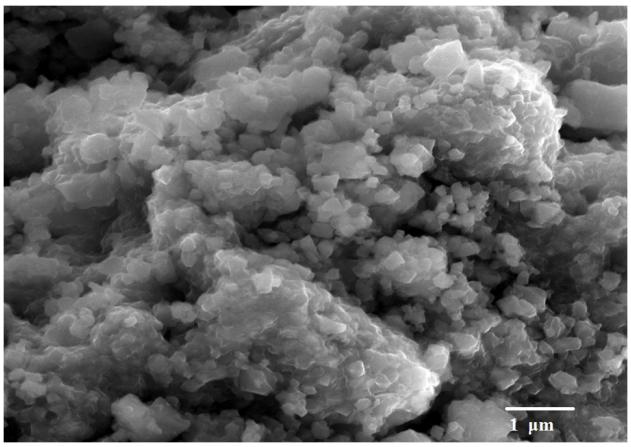

Figure 2. Scanning electron micrograph of $Li(Li_{0.05}Ni_{0.6}Fe_{0.1}Mn_{0.25})O_2$

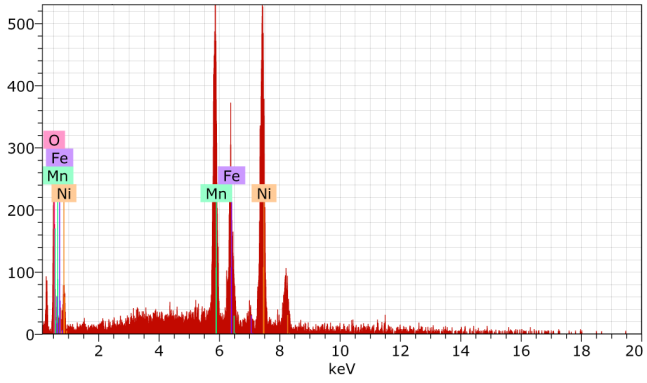

Figure 3. Energy Dispersive Spectrum of $Li(Li_{0.05}Ni_{0.6}Fe_{0.1}Mn_{0.25})O_2$

$$\frac{1}{d^2_{hkl}} = \frac{4}{3}\left[\frac{h^2+hk+k^2}{a^2}\right] + \left[\frac{l^2}{c^2}\right] \quad (2)$$

The unit cell is the parallelepiped built on the vectors, a, b, c, of a crystallographic basis of the direct lattice. Its volume is given by the scalar triple product, V = (a, b, c) and corresponds to the square root of the determinant of the metric tensor. The volume of unit cell (V) is calculated using the following Eq (3).

$$V = \frac{\sqrt{3}a^2c}{2} \quad (3)$$

The crystallite size of the prepared samples is calculated using Debye - Scherrer's formula as given in Eq. (4).

$$D = \frac{0.9\lambda}{\beta cos\theta} \quad (4)$$

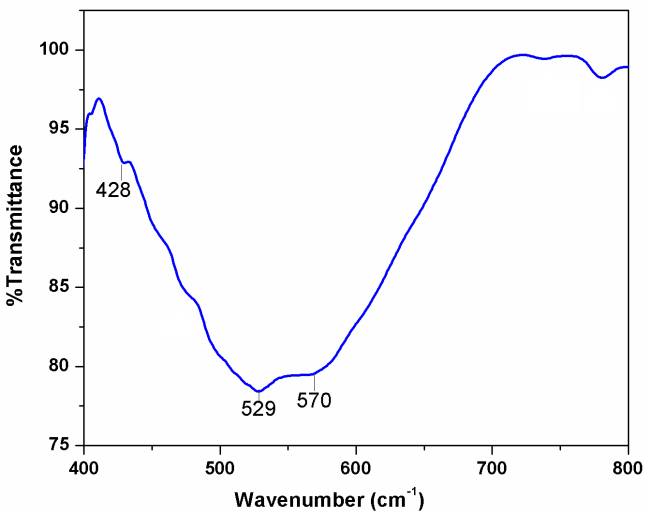

Figure 4. FTIR spectrum of $Li(Li_{0.05}Ni_{0.6}Fe_{0.1}Mn_{0.25})O_2$

Where λ is the wavelength of X-ray used, which is CuKα radiation (λ= 1.5406 Å), and β is the full width at half- maximum of the diffraction peak corresponding to 2θ. Using the above equation the sizes of the crystallites are found to be nano sized crystallites. The crystallite size calculated using the Debye Scherrer formula is about 45 nm.

The surface morphology of cathode materials have been explored and identified by scanning electron microscopy. SEM image of $Li(Li_{0.05}Ni_{0.6}Fe_{0.1}Mn_{0.25})O_2$ is presented in Figure 2. The particles appeared like the small stones remains separately in some region and find to be agglomerated in the other regions. Furthermore, the particles are found to be formed in different sizes mostly in the ramp of 200-250 nm. Figure 3 shows the EDX spectrum of the compound. The presence of emission lines Ni, Mn, Fe and O in the investigated energy range indicates the formation of $Li(Li_{0.05}Ni_{0.6}Fe_{0.1}Mn_{0.25})O_2$ compound. The absence of lithium ion in the spectra indicates the low atomic ratio of lithium[23].

3.2.1. FTIR spectroscopic analysis

The FTIR spectrum in the range of 400-800 cm^{-1} for the synthesized $Li(Li_{0.05}Ni_{0.6}Fe_{0.1}Mn_{0.25})O_2$ material is illustrated in figure 4. The peak observed at 570 cm^{-1} is attributed to O-M-O bending modes and this may mask the characteristic peak of asymmetric M-O stretch which is actually found at 660 cm^{-1} (M = Ni/Fe/Mn). Further, the peak obtained at 529 cm^{-1} may correspond to Li-O stretch which suggests the presence of lithium in the material. The less intense peaks observed at 428 cm^{-1} could be allocated to weak inter metallic interaction between any two metals present in the material [24]. The corresponding peaks mentioned in figure 4 are also correlated with the values of Fe-O stretching and bending modes. Besides, a band at 271 cm^{-1} is also expected [25] but it is not found in the spectra because such lower region is not covered in the present study.

3.2.2. Raman Spectroscopic analysis

The Raman Spectrum of $Li(Li_{0.05}Ni_{0.6}Fe_{0.1}Mn_{0.25})O_2$ compound is

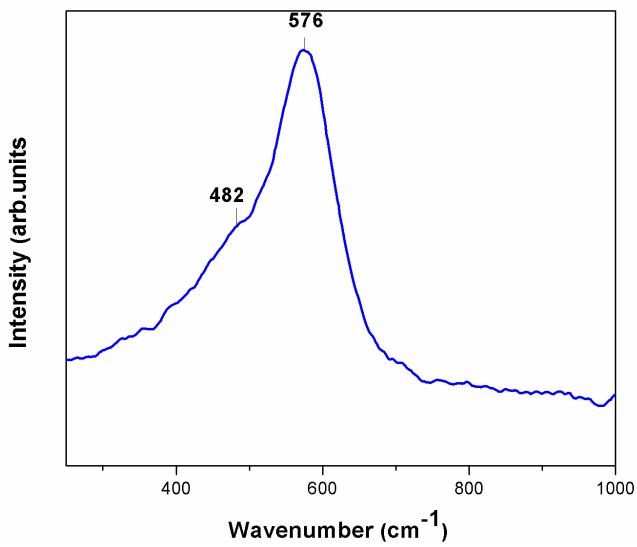

Figure 5. Raman spectrum of $Li(Li_{0.05}Ni_{0.6}Fe_{0.1}Mn_{0.25})O_2$

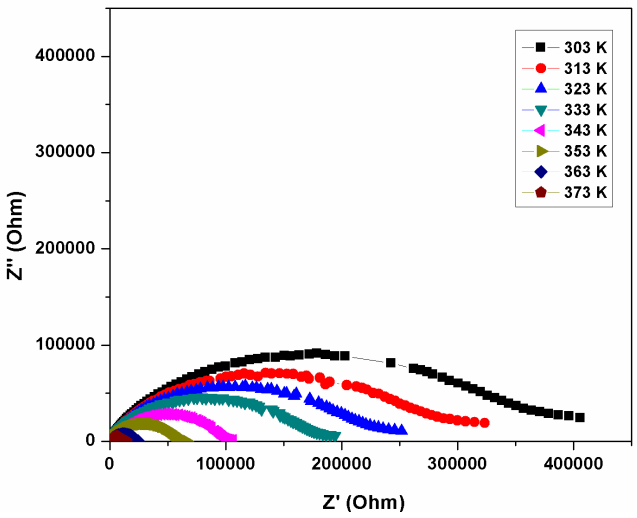

Figure 6. Cole-Cole impedance plot of $Li(Li_{0.05}Ni_{0.6}Fe_{0.1}Mn_{0.25})O_2$ at different temperatures

presented in figure 5. For the layered structure cathode material with a space group R $\bar{3}$ m is similar to the compound $LiCoO_2$. Therefore, the corresponding optical vibration modes are:

$\Gamma = A_{2g}+E_g+2A_{2u}+2E_u$ [14]. The first two modes are visible only by Raman while the second two modes can be visible by IR. Theoretically, two Raman bands and four IR bands should be visible for the layer structured material with space group R $\bar{3}$ m. Figure 5 shows the peaks around which are the corresponding active M-O symmetrical stretching and bending vibrational Raman modes of A_{1g} and E_g.

3.3. Impedance spectroscopic analysis

The ionic conductivity of the prepared $Li(Li_{0.05}Ni_{0.6}Fe_{0.1}Mn_{0.25})O_2$ was calculated by means of the following Eq.(5).

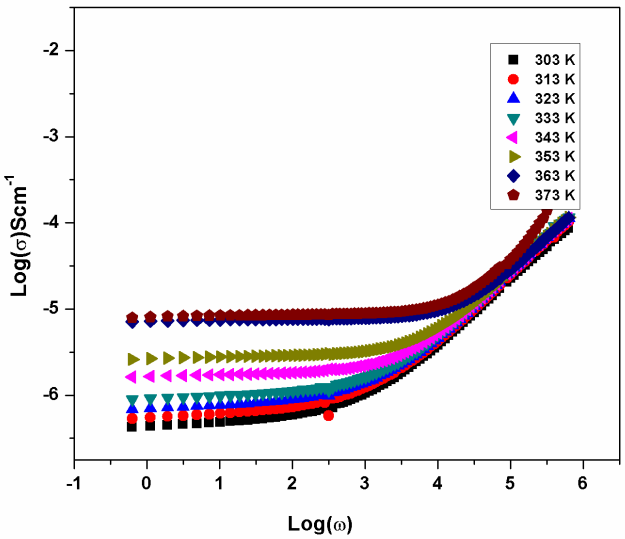

Figure 7. Logarithm of ω Vs logarithm of σ for $Li(Li_{0.05}Ni_{0.6}Fe_{0.1}Mn_{0.25})O_2$

$$\sigma = \frac{t}{R_b A} \tag{5}$$

Where t and A are the thickness and area of the $Li(Li_{0.05}Ni_{0.6}Fe_{0.1}Mn_{0.25})O_2$ in contact with the gold blocking electrodes respectively. Thickness of the $Li(Li_{0.05}Ni_{0.6}Fe_{0.1}Mn_{0.25})O_2$ was measured by means of micrometer screw gauge. R_b represents the bulk resistance, which is obtained from extrapolation of semicircular region to highest frequencies. Figure 6 represents the cole-cole impedance plot of $Li(Li_{0.05}Ni_{0.6}Fe_{0.1}Mn_{0.25})O_2$. It is inferred from the plot that at high frequencies a compressed semicircle was obtained. This may due to distribution of relaxation times. The graph between logarithm of frequency Vs conductivity at various temperatures for $Li(Li_{0.05}Ni_{0.6}Fe_{0.1}Mn_{0.25})O_2$ is shown in Figure 7. It is observed from Figure 7 that ionic conductivity increases with increase in temperature. The ionic conductivity of $Li(Li_{0.05}Ni_{0.6}Fe_{0.1}Mn_{0.25})O_2$ obeys the Arrhenius law of conduction mechanism.

$$\sigma = \sigma_0 A e^{-E_a/kT} \tag{6}$$

Where A and K are constants. E_a is the activation energy of the sample. It is calculated from the slope of the linear fit of the Arrhenius plot and its value is found to be 0.29 eV from Figure 8. Further, the increase in ionic conductivity is also due to the availability of conducting ions in the material[26-28]. It is inferred from Figure 6 that, the maximum ionic conductivity of prepared sample is found to be in the range of $7.9x10^{-6}$ S/cm. This result is different from the previously reported values such as $10^{-3.4}$S/cm for $Li(Li_{0.05}Ni_{0.4}Co_{0.3}Mn_{0.25})O_2$ [24] and 10^{-4}S/cm for$LiCoO_2$ [29].

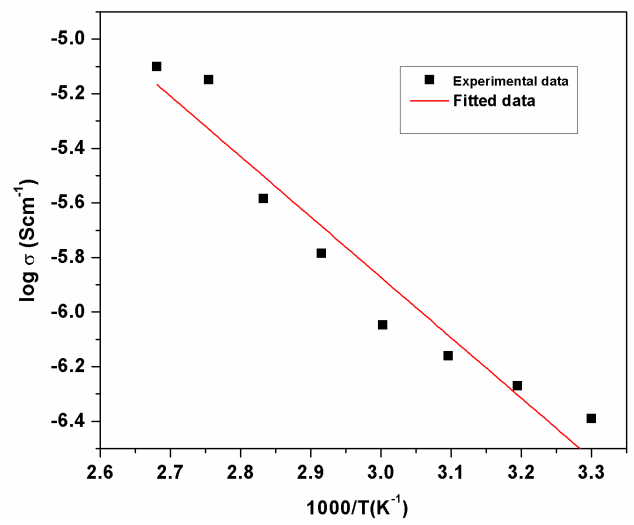

Figure 8. Arrhenius plot of $Li(Li_{0.05}Ni_{0.6}Fe_{0.1}Mn_{0.25})O_2$

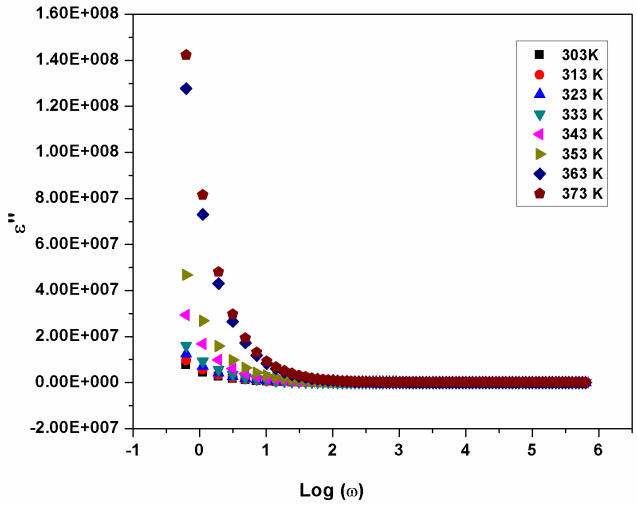

Figure 9. Logarithm of ω versus dielectric loss ε'' at different temperatures for $Li(Li_{0.05}Ni_{0.6}Fe_{0.1}Mn_{0.25})O_2$

3.4. Dielectric spectra analysis

Dielectric spectra analysis is an important tool, which provides enough information about the conduction phenomena. The dielectric property acts as an indicator to prove that the increase in ionic conductivity is due to increase in charge carriers[30-32]. Also, it indicates the amount of charge that can be stored by a material. A wide frequency dielectric relaxation spectroscopy is a tool to study the relaxation of dipoles. The complex permittivity ε* or dielectric constant of a system is evaluated by means of the following expression.

$$\varepsilon^* = \varepsilon' - j\varepsilon'' \tag{7}$$

Where ε' is the real part of dielectric constant and ε" is the imaginary part of dielectric constant of the material.

$$\varepsilon' = \frac{cd}{\varepsilon_0 A} \tag{8}$$

$$\varepsilon'' = \frac{\sigma'}{\omega\varepsilon_0} \tag{9}$$

Where σ' is the real part of conductivity (S/cm), C is the parallel capacitance (F); d (cm) and A (cm^2) are thickness and area of the pelletized $Li(Li_{0.05}Ni_{0.6}Fe_{0.1}Mn_{0.25})O_2$, ω the angular frequency and ε_o is the permittivity of free space which is equal to 8.856x 10^{-14} F/cm. Figure 9 represents the variation of ε'' as a function of log frequency for $Li(Li_{0.05}Ni_{0.6}Fe_{0.1}Mn_{0.25})O_2$ at different temperatures. The dispersion of dielectric constant is high at low frequency for all temperatures and this may be attributed to the formation of space charge polarization at the electrode interface, where the space charge regions with respect to the frequency are explained in terms of ion diffusion. At higher frequencies the change in the direction of the electric field lines is too fast to be followed by the charged ions and hence the dielectric constant decreases. From figure 9 it is identified that the dielectric constant increases with increase in temperature.

4. CONCLUSIONS

$Li(Li_{0.05}Ni_{0.6}Fe_{0.1}Mn_{0.25})O_2$ cathode material was prepared using sol-gel method with citric acid as chelating agent. The cathode material possessed similar structure of hexagonal α–$NaFeO_2$ structure that was confirmed from XRD pattern. The occurrence of all the elements in the cathode material was pre-determined and it was confirmed by EDS. The prepared material possessed an excellent electrical property, which was observed from ionic conductivity analysis. The maximum ionic conductivity was found to be in the order of 10^{-6} S/cm. The higher value of dielectric constant with increase in temperature represented the increase in polarizability in the material. This result strongly supports the results obtained in ionic conductivity analysis.

REFERENCES

[1] J.-M. Tarascon, M. Armand, Nature, 414, 359 (2001).
[2] D.K. K. Karuppasamy, Yong Hee Kang, K. Prasanna, Hee Woo Rhee, J. Indust. and Engi Chem., http://dx.doi.org/10.1016/j.jiec.2017.03 (2017).
[3] H.W.R. K. Karuppasamy, P. Anil Reddy, Dipti Gupta, Liviu Mitu, Anji Reddy Polu, X. Sahaya Shajan, J. of Indust. and Engi. Chem., DOI: 10.1016/j.jiec.2016.06.020 (2016).
[4] H.-S.K. K. Karuppasamy, Dongkyu Kim, Dhanasekaran Vikraman, K. Prasanna, A.Kathalingam, Ramakant Sharma, Hee Woo Rhee, Scientific Reports, (10.1038/s41598-017-11614-1) 11103 (2017).
[5] J.W. Fergus, J. Power Sources, 195, 939 (2010).
[6] M.S. Whittingham, Chem. review, 104, 4271 (2004).
[7] A. Nichelson, S. Karthickprabhu, K. Karuppasamy, G. Hirankumar, X. Sahaya Shajan, Mater. Focus 5 324, (2016).

[8] S Karthickprabhu, G Hirankumar, A Maheswaran, C Sanjeeviraja, J. Alloys and Compds., 548, 65 (2013).
[9] T. Ohzuku, M. Nagayama, K. Tsuji, K. Ariyoshi, Journal of Materials chemistry, 21, 10179 (2011).
[10]S Karthickprabhu, G Hirankumar, Int J ChemTech Res, 6, 5256 (2014).
[11]H. Yoshizawa, T. Ohzuku, J. Power Sources, 174, 813 (2007).
[12]S Karthickprabhu, G Hirankumar, A Maheswaran, RSD Bella, C Sanjeeviraja, Ionics, 21, 345 (2015).
[13]Y. Koyama, I. Tanaka, H. Adachi, Y. Makimura, T. Ohzuku, J. Power Sources, 119, 644 (2003).
[14]T. Ohzuku, Y. Makimura, Chemistry Letters, 30, 744 (2001).
[15]H. Tang, F. Zhao, Z.-r. Chang, X.-Z. Yuan, H. Wang, Journal of The Electrochemical Society, 156, A478 (2009).
[16]N.N. Sinha, N. Munichandraiah, ACS applied materials & interfaces, 1, 1241 (2009).
[17]C.-C. Wang, A. Manthiram, Journal of Mater. Chem. A, 1, 10209 (2013).
[18]A. Rougier, I. Saadoune, P. Gravereau, P. Willmann, C. Delmasa, Solid State Ionics, 90, 83 (1996).
[19]B. Hwang, R. Santhanam, D. Liu, J. power sources, 97, 443 (2001).
[20]S.K. Jeong, C.-H. Song, K.S. Nahm, A.M. Stephan, Electrochim. Acta, 52, 885 (2006).
[21]J.-H. Kim, C. Park, Y.-K. Sun, Solid State Ionics, 164, 43 (2003).
[22]S. Thanikaikarasan, T. Mahalingam, K. Sundaram, A. Kathalingam, Y.D. Kim, T. Kim, Vacuum, 83, 1066 (2009).
[23]X. Jin, Q. Xu, X. Yuan, L. Zhou, Y. Xia, Electrochim. Acta, 114, 605 (2013).
[24]A. Nichelson, S. Thanikaikarasan, Pratap Kollu, P.J. Sebastian, T. Mahalingam and X.Sahaya Shajan, J. New Mat. Electr. Sys. 17, 153 (2014).
[25]P. Suresh, S. Rodrigues, A. Shukla, H. Vasan, N. Munichandraiah, Solid State Ionics, 176, 281 (2005).
[26]K. Karuppasamy, C.V. Vani, R. Antony, S. Balakumar, X.S. Shajan, Polymer Bulletin 70, 2531 (2013).
[27]K. Karuppasamy, C.V. Vani, A. Nichelson, S. Balakumar, X.S. Shajan, Effect of nanochitosan and succinonitrile on the AC ionic conductivity of plasticized nanocomposite solid polymer electrolytes (PNCSPE), AIP Conference Proceedings, AIP 845 (2013).
[28]C. Ambika , G.Hirankumar, S. Karthickprabhu, R. S. Daries Bella, , Int J ChemTech Res, 6, 5209 (2014).
[29]B.N. Rao, M. Venkateswarlu, N. Satyanarayana, Ionics, 20, 175 (2014).
[30]K. Karuppasamy, T. Linda, S. Thanikaikarasan, S. Balakumar, T. Mahalingam, P. Sebastian, X. Sahaya Shajan, J. New Mat. Electr. Sys., 16, 116 (2013).
[31]K. Karuppasamy, S. Thanikaikarasan, S. Balakumar, P. Thiravetyan, D. Eapen, P. Sebastian, X.S. Shajan, J. New Mat. Electr. Sys., 16, 2 (2013).
[32]S Karthickprabhu, G Hirankumar, S Thanikaikarasan, PJ Sebastian, J. New Mat. Electr. Sys., 17, 159 (2014).
[33]RS Daries Bella, S Karthickprabhu, A Maheswaran, C Amibika, G Hirankumar, Premanand Devaraj, Physica B: Condensed Matter, 458, 51 (2015).